Comparison of three widely used multi-GNSS real-time single-frequency precise point positioning models using the International GNSS Service real-time service

Ahao Wang[1,2], Junping Chen[2,3,4] ✉, Yize Zhang[2,5], Jiexian Wang[1]

[1]College of Surveying and Geo-Informatics, Tongji University, Shanghai, 200092, People's Republic of China
[2]Shanghai Astronomical Observatory, Chinese Academy of Sciences, Shanghai, 200030, People's Republic of China
[3]School of Astronomy and Space Science, University of Chinese Academy of Sciences, Beijing, 100049, People's Republic of China
[4]Shanghai Key Laboratory of Space Navigation and Positioning Techniques, Shanghai Astronomical Observatory, Chinese Academy of Sciences, Shanghai, 200030, People's Republic of China
[5]Tokyo University of Marine Science and Technology, Tokyo, 1358533, Japan
✉ E-mail: junping@shao.ac.cn

Abstract: Real-time single-frequency precise point positioning (RT-SFPPP) of low-cost has been attracting increasing attention in numerous global navigation satellite system (GNSS) applications. Nowadays, three multi-GNSS RT-SFPPP models are widely applied, i.e. ionosphere-corrected (IC), ionospherefree (IF) and ionosphere-weighted (IW) models. A comprehensive evaluation of the three models using CLK93 products is performed in the aspect of observation residuals, positioning accuracy and convergence. Data sets with quad-system are collected from 16 multi-GNSS experiments (MGEX) stations and are analysed in the simulated kinematic precise point positioning (PPP). Besides, kinematic PPP for a 5-h shipborne data set is also conducted. Experimental results show that the positioning accuracy of IW model using MGEX data is better than that of both IC and IF models. Regarding the kinematic shipborne test, positioning accuracy of IF/IW model is of 0.27/0.26, 0.21/0.26 and 0.49/0.48 m for the N, E and U components, respectively, which is much better than that of IC model. As for average convergence time, IW model shows the best performance, which is at least 25% faster than the IF model. Different from both IF and IW models, the amplification of ionospheric errors has some impact on the positioning performance of the IC model at different frequencies.

1 Introduction

In order to meet the requirements of real-time high-precision global navigation satellite system (GNSS) applications, the International GNSS Service (IGS) set up a real-time working group in 2001 [1] and has been officially providing an open-access real-time service (RTS) since 1 April 2013 [2]. RTS products include GNSS satellite orbit and clock corrections and support real-time dual-frequency precise point positioning (RT-DFPPP) to achieve centimetre- to decimetre-level accuracy [3, 4]. In most positioning, navigation and timing services, GNSS users tend to use the low-cost but high-precision devices tracking only single-frequency signals. Therefore, real-time single-frequency precise point positioning (RT-SFPPP) has begun attracting more and more attention in the booming GNSS markets [5, 6].

Ionospheric delay error is one of the largest error sources of RT-SFPPP and needs to be properly dealt with. Several available broadcast ionospheric models, i.e. Klobuchar, NeQuick, BeiDou global broadcast ionospheric delay correction model (BDGIM) and Neustrelitz total electron content broadcast model (NTCM-BC), can be applied to mitigate the ionospheric effect in RT-SFPPP, but they could correct only for 50–75% of the ionospheric errors on the global scale [7–12]. Advancing real-time high accuracy GNSS applications, the Center National d'Etudes Spatiales (CNES) provides real-time ionospheric vertical total electron content (VTEC) through the RTS stream CLK93 together with other corrections (i.e. orbit, clock, code bias and carrier-phase bias). Compared with the IGS final global ionospheric map products, the root mean square (RMS) of CNES VTEC products is about 1–3 total electron content units (TECUs) [13]. Such precise ionospheric products can be applied to the ionosphere-corrected (IC) RT-SFPPP model, but it can only achieve sub-metre-level horizontal and metre-level vertical kinematic positioning solutions. Liu *et al*. [14]

introduced the CNES VTEC products into the ionosphere-weighted (IW) RT-SFPPP, where the kinematic precise point positioning (PPP) convergence time is reduced and decimetre-level positioning accuracy can be derived. However, this contribution is only followed by the interest that the performance of GPS and Galileo in the simulated kinematic solution and lack the 'true' RT kinematic positioning results using quad-system observations. In addition, the GRoup And PHase Ionospheric Correction (GRAPHIC) model can be formulated in RT-SFPPP, which is free of ionospheric delay errors using the average of code and phase [15, 16]. Although this model can achieve a satisfying positioning accuracy, it generally needs long convergence time [17, 18]. The performance of ionosphere-free (IF) SFPPP model using IGS RTS also needs to be investigated.

Using RTS orbit and clock corrections, most of the previous studies mainly concentrated on the validation and numerical performance of RT-DFPPP. As for RT-SFPPP, there are only a few contributions related to the IC or IW model for the single or dual system (e.g. GPS + Globalnaya Navigatsionnaya Sputnikovaya Sistema (GLONASS), GPS + Galileo). So far, no analysis was reported regarding the comparisons of IC, IF and IW RT-SFPPP models using quad-system (GPS + GLONASS + BDS-2 + Galileo) observations and the CNES VTEC products. In this paper, we focus on the comparison of three widely used multi-GNSS RT-SFPPP models in terms of observation residual, kinematic positioning accuracy and convergence time.

This contribution is organised as follows. Section 1 formulates three RT-SFPPP models of quad-system observations. Then, the quality of RTS orbit and clock corrections provided by the CLK93 stream is evaluated in Section 2. In Section 3, the observation residuals, positioning accuracy and convergence time of multi-GNSS RT-SFPPP in the kinematic mode with multi-GNSS experiment (MGEX) stations are analysed. Furthermore, a true RT

kinematic test is carried out to investigate the performance of three RT-SFPPP models in Section 4. Finally, the research findings and conclusions are summarised in Section 5.

2 Methodology for multi-GNSS real-time single-frequency PPP

2.1 General GNSS RT-SFPPP model

The basic undifferenced and uncombined observation equations of the GNSS code P and carrier phase L can be expressed as [19]

$$P_{i,k}^s = \rho_k^s + dt_{r,k} - dt_k^s + d\theta_k^s + T_k^s + \mu_i \cdot I_i^s + D_i - d_i^s + \varepsilon_{p_k}$$
$$L_{i,k}^s = \rho_k^s + dt_{r,k} - dt_k^s + d\theta_k^s + T_k^s - \mu_i \cdot I_i^s + B_i - b_i^s - N_i^s + \varepsilon_{L_k} \tag{1}$$

where the subscripts i and k denote the frequency and epoch, the superscript 's' denotes the satellite. ρ_k^s is the computed geometric range between the satellite and receiver. $dt_{r,k}$ and dt_k^s are the clock errors of receiver and satellite. $d\theta_k^s$ is the satellite orbit errors, T_k^s is the slant tropospheric delay, I_k^s is the slant ionospheric delay at the first frequency and $\mu_i = f_1^2/f_i^2$ with f_i being the ith frequency. B_i and D_i are the hardware delays of phase and code for receiver, while b_i^s and d_i^s are the hardware delays of phase and code for satellite. N_i^s is the integer phase ambiguity, absorbing the initial phase biases of both receiver and satellite. ε_{p_k} and ε_{L_k} are the measurement noise of code and phase.

In (1), satellite orbit and clock errors can be corrected using the products from the RTS CLK93 stream. The CLK93 products are generated using the IF observables, and the satellite clock corrections dt_{IF} contains the IF combination of the code hardware delays and can be defined as [18]

$$dt_{IF}^s = dt^s + \frac{f_1^2}{f_1^2 - f_2^2}d_1^s - \frac{f_2^2}{f_1^2 - f_2^2}d_2^s$$
$$= dt^s + d_1^s - \frac{f_2^2}{f_1^2 - f_2^2}DCB_{12}^s \tag{2}$$

where $DCB_{12}^s = d_2^s - d_1^s$ is the between-frequency satellite differential code bias (DCB) that is obtained from CLK93 bias products and therefore the satellite clock dt^s in (1) can be derived as

$$dt^s = dt_{IF}^s - d_1^s + \frac{f_2^2}{f_1^2 - f_2^2}DCB_{12}^s \tag{3}$$

Considering IF satellite orbit and clock corrections and (3), (1) can be re-written as

$$P_{i,k}^s = \rho_k^s + dt_{r,k} + T_k^s + \mu_i \cdot I_i^s + D_i - d_i^s + d_1^s + \varepsilon_{p_k}$$
$$L_{i,k}^s = \rho_k^s + dt_{r,k} + T_k^s - \mu_i \cdot I_i^s + B_i - b_i^s + d_1^s - N_i^s + \varepsilon_{L_k} \tag{4}$$

Thus, epoch-wise observation equations of s-satellites of first frequency can be expressed as

$$P_k = A_k x_k + e_s \cdot dt_{r,k} + M_k \cdot ZWD + I_k + D_1 + \varepsilon_{p_k}$$
$$L_k = A_k x_k + e_s \cdot dt_{r,k} + M_k \cdot ZWD - I_k + B_1 - b_1 + d_1 - N_1 + \varepsilon_{L_k} \tag{5}$$

where $P_k = [P_k^1, ..., P_k^s]^T$ and $L_k = [L_k^1, ..., L_k^s]^T$ are the vectors of epoch-wise code and phase observations. A_k is the unit vector of the satellite and receiver, e_s is the unit vector. x_k is the receiver position vectors. ZWD is the residual zenith tropospheric delay with the elevation-dependent mapping coefficient vector $M_k = [M_k^1, ..., M_k^s]^T$. $I_k = [I_k^1, ..., I_k^s]^T$ and $N_1 = [N_1^1, ..., N_1^s]^T$ are the vectors of slant ionospheric delays and ambiguities.

$b_1 = [b_1^1, ..., b_1^s]^T$ and $d_1 = [d_1^1, ..., d_1^s]^T$ are the vectors of satellite phase and code hardware delays, $B_1 = [B_1^1, ..., B_1^s]^T$ and $D_1 = [D_1^1, ..., D_1^s]^T$ are the vectors of receiver phase and code hardware delays.

It should be noted that the receiver hardware delays of code D_1 and phase B_1 are frequency-dependent, thus the receiver hardware delays are common terms for all satellites of the division multiple access (CDMA) system (i.e. GPS, Galileo and BDS) in (5). Rank deficiency due to parameter correlations exists in (5), thus receiver pseudo-range delay is normally grouped with receiver clocks and ambiguities will be biased consequently. The coupled receiver clock $d\bar{t}_{r,k}$ and ambiguity $\bar{N}$ are defined as

$$d\bar{t}_{r,k} = \begin{cases} dt_{r,k} + D_1, & \text{for CDMA} \\ dt_{r,k} + D_1^1, & \text{for FDMA} \end{cases} \tag{6}$$

$$\bar{N} = \begin{cases} N_1 + (b_1 - d_1) - e_s(B_1 - D_1), & \text{for CDMA} \\ N_1 + (b_1 - d_1) - B_1 + e_sD_1^1, & \text{for FDMA} \end{cases} \tag{7}$$

In the (6), D_1 is the receiver code hardware delay of the CDMA system, while D_1^1 is the receiver code hardware delay of the first satellite for the frequency division multiple access system (i.e. GLONASS). Satellite-related hardware delays are mitigated into ambiguity. According to (6), the receiver hardware delays of first GLONASS satellites are ground with receiver clocks, and the receiver hardware delays of other GLONASS satellites have to be estimated in the term of inter-frequency code biases (IFCB) $\delta D = [D_1^2 - D_1^1, ..., D_1^s - D_1^1]^T$. Linear IFCB function of channel number as the parameter is used in this study [20].

Applying the above definitions, the single-system RT-SFPPP function model can be expressed as

$$P_k = A_k x_k + e_s \cdot d\bar{t}_{r,k} + M_k \cdot ZWD + I_k + \delta D + \varepsilon_{p_k}$$
$$L_k = A_k x_k + e_s \cdot d\bar{t}_{r,k} + M_k \cdot ZWD - I_k - \bar{N} + \varepsilon_{L_k} \tag{8}$$

2.2 IC RT-SFPPP model

Another key issue in RT-SFPPP is the ionospheric delay handling. In IC RT-SFPPP model, ionospheric delays are corrected by external ionosphere models. However, due to the errors of external ionospheric models, the IC RT-SFPPP model usually leads to the biased solutions [21]. In this study, the CNES VTEC products are used in IC RT-SFPPP model. Extending the RT-SFPPP model to quad-system (GPS + GLONASS + BDS + Galileo), the multi-GNSS RT-SFPPP based on the IC model is as follows

$$\begin{cases} P_k^G = A_k^G x_k + e_s \cdot d\bar{t}_{r,k}^G + M_k^G \cdot ZWD + \varepsilon_{P_k}^G \\ P_k^R = A_k^R x_k + e_s \cdot d\bar{t}_{r,k}^G + ISB_k^R + M_k^R \cdot ZWD + \delta D + \varepsilon_{P_k}^R \\ P_k^C = A_k^C x_k + e_s \cdot d\bar{t}_{r,k}^G + ISB_k^C + M_k^C \cdot ZWD + \varepsilon_{P_k}^C \\ P_k^E = A_k^E x_k + e_s \cdot d\bar{t}_{r,k}^G + ISB_k^E + M_k^E \cdot ZWD + \varepsilon_{P_k}^E \end{cases} \tag{9a}$$

$$\begin{cases} L_k^G = A_k^G x_k + e_s \cdot d\bar{t}_{r,k}^G + M_k^G \cdot ZWD - \bar{N}_k^G + \varepsilon_{L_k}^G \\ L_k^R = A_k^R x_k + e_s \cdot d\bar{t}_{r,k}^G + ISB_k^R + M_k^R \cdot ZWD - \bar{N}_k^R + \varepsilon_{L_k}^R \\ L_k^C = A_k^C x_k + e_s \cdot d\bar{t}_{r,k}^G + ISB_k^C + M_k^C \cdot ZWD - \bar{N}_k^C + \varepsilon_{L_k}^C \\ L_k^E = A_k^E x_k + e_s \cdot d\bar{t}_{r,k}^G + ISB_k^E + M_k^E \cdot ZWD - \bar{N}_k^E + \varepsilon_{L_k}^E \end{cases} \tag{9b}$$

where the superscript G, R, C and E denote the GPS, GLONASS, BDS and Galileo, respectively. The receiver clock is based on GPS signals and inter-system biases (ISBs) $ISB = [ISB^1, ..., ISB^s]^T$ are introduced to compensate system time offsets [22–25]. The parameter vector X can be expressed as

$$X = [x, d\bar{t}_r^G, ISB, ZWD, \delta D, \bar{N}] \tag{10}$$

2.3 IF RT-SFPPP model

Propagation delays caused by ionosphere between a satellite and a station have an opposite sign for code and phase observations, the GRAPHIC linear IF combination is extensively used in RT-SFPPP. Although high-precision solutions can be achieved since the ionospheric error is completely removed, long convergence time is required due to the large noise of the IF observables. It is worth noting that the code observables ((9a)) are required in IF model to avoid the rank deficiency and the ionospheric delay is corrected by the CNES VTEC products for code observations. The multi-GNSS IF RT-SFPPP model can be expressed as

(see (11))

The parameter vector X of multi-GNSS IF RT-SFPPP can be expressed as

$$X = \left[x, \mathrm{d}\bar{t}_r^G, \mathrm{ISB}, \mathrm{ZWD}, \frac{\delta D}{2}, \frac{\bar{N}}{2} \right] \tag{12}$$

2.4 IW RT-SFPPP model

The ionospheric delay can also be estimated as an unknown parameter in RT-SFPPP. Many studies have proved that the IF model of eliminating ionospheric delays is equivalent to estimating the ionospheric delay parameters without constraints [18, 26]. In this approach, external ionospheric corrections are regarded as virtual observation equation with constraints, i.e. $\tau_k = I_k + \varepsilon_{\tau_k}$ with τ_k being the priori ionospheric correction. The constraints of virtual ionospheric corrections have big effect on positioning performance, we use the CNES VTEC products in this study and their variances can be defined by the (17) in [27]. Therefore, multi-GNSS IW RT-SFPPP can be expressed as

$$\begin{cases} P_k^G = A_k^G x_k + e_s \cdot \mathrm{d}\bar{t}_{r,k}^G + M_k^G \cdot \mathrm{ZWD} + I_k^G + \varepsilon_{P_k}^G \\ P_k^R = A_k^R x_k + e_s \cdot \mathrm{d}\bar{t}_{r,k}^G + \mathrm{ISB}_k^R + M_k^R \cdot \mathrm{ZWD} + I_k^R + \delta D + \varepsilon_{P_k}^R \\ P_k^C = A_k^C x_k + e_s \cdot \mathrm{d}\bar{t}_{r,k}^G + \mathrm{ISB}_k^C + M_k^C \cdot \mathrm{ZWD} + I_k^C + \varepsilon_{P_k}^C \\ P_k^E = A_k^E x_k + e_s \cdot \mathrm{d}\bar{t}_{r,k}^G + \mathrm{ISB}_k^E + M_k^E \cdot \mathrm{ZWD} + I_k^E + \varepsilon_{P_k}^E \end{cases} \tag{13a}$$

$$\begin{cases} L_k^G = A_k^G x_k + e_s \cdot \mathrm{d}\bar{t}_{r,k}^G + M_k^G \cdot \mathrm{ZWD} - I_k^G - \bar{N}_k^G + \varepsilon_{L_k}^G \\ L_k^R = A_k^R x_k + e_s \cdot \mathrm{d}\bar{t}_{r,k}^G + \mathrm{ISB}_k^R + M_k^R \cdot \mathrm{ZWD} - I_k^R - \bar{N}_k^R + \varepsilon_{L_k}^R \\ L_k^C = A_k^C x_k + e_s \cdot \mathrm{d}\bar{t}_{r,k}^G + \mathrm{ISB}_k^C + M_k^C \cdot \mathrm{ZWD} - I_k^C - \bar{N}_k^C + \varepsilon_{L_k}^C \\ L_k^E = A_k^E x_k + e_s \cdot \mathrm{d}\bar{t}_{r,k}^G + \mathrm{ISB}_k^E + M_k^E \cdot \mathrm{ZWD} - I_k^E - \bar{N}_k^E + \varepsilon_{L_k}^E \end{cases} \tag{13b}$$

$$\tau_k = I_k + \varepsilon_{\tau_k} \tag{13c}$$

The parameter vector X of multi-GNSS IW RT-SFPPP can be expressed as

$$X = \left[x, \mathrm{d}\bar{N}_r^G, \mathrm{ISB}, \mathrm{ZWD}, I, \delta D, \bar{N} \right] \tag{14}$$

Among the three RT-SFPPP models, the IC model is most affected by the ionospheric delay, and it is often used to indirectly access the quality of various ionosphere models.

3 Quality assessment of CLK93 orbit and clock products

Nowadays, five types of CLK93 products, including the satellite orbit/clock corrections, code/phase bias and the VTEC messages, are formatted into state space representation message and are broadcasted through the internet using the networked transport of RTCM-V.3 via internet protocol [28]. The sampling rate of the satellite orbit/clock corrections and code/phase bias is set to 5 s, whereas for the VTEC, the interval is as low as 60 s in the CLK93 stream.

As the performance of multi-GNSS RT-SFPPP depends on the accuracy and reliability of RT orbit and clock products, the product quality of RTS CLK93 stream is evaluated before applied to positioning. Taking the final precise products of GBM released by the Deutsches GeoForschungs Zentrum as reference [29], we analyse the quad-system (GPS + GLONASS + BDS-2 + Galileo) RT orbit and clock products over the period from day of year (DOY) 121 to 130 in 2019. The orbit and clock comparison were performed every 5 min and 30 s according to the intervals of the final products. During the test period, the availability of CLK93 products is about 95.25% and the missing epochs are due to the loss of network connection or caster malfunctioning. The missing RT orbits are replaced by the IGS Ultra-rapid orbits at the same period as they are reported to have the same accuracy [30]. As for RT clocks, they could be predicted using polynomial fittings for a short time [2]. To remove temporal/spatial reference discrepancies between RT and precise products, key issues need to be taken into account: (i) The GBM products refer to the satellite centre of mass, whereas the CLK93 products adopt the antenna phase centre (APC) of the satellite, thus the satellite phase centre offset (PCO) should be corrected using igs14.atx [31] (ii) The clock products of CLK93 and GBM have the different clock datum, a medium GLK93-minus-GBM value of all satellite clocks at each epoch is calculated as a systematic bias to eliminate this difference [32].

Fig. 1 shows the satellite-specific RMS of differences between the CLK93 orbits and the GBM final orbits for quad-system in the radial, along-track and cross-track components. Noted that CLK93 includes BDS products only for the regional system BDS-2, where the geostationary earth orbit satellites (C01–C05) are excluded due to low quality [33]. The orbit accuracy of GPS and Galileo satellites shows a similar level and much better than that of GLONASS and BDS satellites in the three components. For all satellites, the radial component generally presents a better agreement with the final orbits than those in the cross-track component, while the agreement in the along-track component is the worst. However, there is an exception for GLONASS-K R09 satellite, whose orbit accuracy in the radial component is >20 cm and thus is rejected in the following positioning experiments. The average RMS values of all satellites in orbit errors for each system are summarised in Table 1. For GPS/Galileo satellites, the RMS values for CLK93 orbits are <3/3.5 cm in the radial and cross-track components and <4/4.5 cm in the along-track component. The RMS of GLONASS satellite orbits reaches up to 4.36, 11.34 and 7.37 cm in the radial, along-track and cross-track components, respectively, which are close to the results as reported by [33–34]. Due to the limitation of BDS-2 tracking network, BDS-2 satellites (C06-C14) orbits have the worst performance in all systems.

Different from the orbit assessment, the standard derivation (STD) value will generally be taken as the indicator for evaluating the clock quality since the removed mean biases can be absorbed

$$\begin{cases} \dfrac{P_k^G + L_k^G}{2} = A_k^G x_k + e_s \cdot \mathrm{d}\bar{t}_{r,k}^G + M_k^G \cdot \mathrm{ZWD} - \dfrac{\bar{N}_k^G}{2} + \dfrac{\varepsilon_{P_k}^G + \varepsilon_{L_k}^G}{2} \\[2mm] \dfrac{P_k^R + L_k^R}{2} = A_k^R x_k + e_s \cdot \mathrm{d}\bar{t}_{r,k}^G + \mathrm{ISB}_k^R + M_k^R \cdot \mathrm{ZWD} + \dfrac{\delta D}{2} - \dfrac{\bar{N}_k^R}{2} + \dfrac{\varepsilon_{P_k}^R + \varepsilon_{L_k}^R}{2} \\[2mm] \dfrac{P_k^C + L_k^C}{2} = A_k^C x_k + e_s \cdot \mathrm{d}\bar{t}_{r,k}^G + \mathrm{ISB}_k^C + M_k^C \cdot \mathrm{ZWD} - \dfrac{\bar{N}_k^C}{2} + \dfrac{\varepsilon_{P_k}^C + \varepsilon_{L_k}^C}{2} \\[2mm] \dfrac{P_k^E + L_k^E}{2} = A_k^E x_k + e_s \cdot \mathrm{d}\bar{t}_{r,k}^G + \mathrm{ISB}_k^E + M_k^E \cdot \mathrm{ZWD} - \dfrac{\bar{N}_k^E}{2} + \dfrac{\varepsilon_{P_k}^E + \varepsilon_{L_k}^E}{2} \end{cases} \tag{11}$$
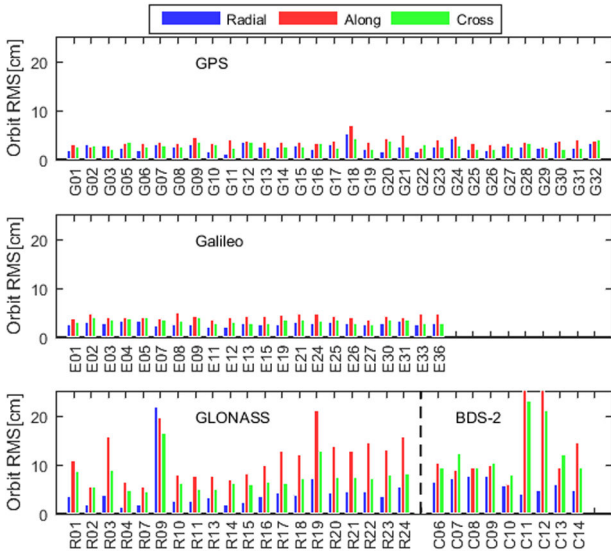
Fig. 1 *RMS values of the differences between CLK93 orbits and GBM final orbits for the GPS, GLONASS, BDS-2 and Galileo in the radial, along-track and cross-track components*

Table 1 Average RMS/STD values of CLK93 orbit/clock errors with respect to GBM final products for quad-system in a 14-day test period

System	RMS			STD
	R, cm	A, cm	C, cm	T, ns
GPS	2.59	3.61	2.75	0.10
GLONASS	4.36	11.34	7.37	0.22
BDS-2	6.00	14.71	12.74	0.30
Galileo	2.74	4.24	3.29	0.10

The variables 'R', 'A', 'C' and 'T' denote the orbit errors of radial, along-track and cross-track as well as clock errors, respectively

by ambiguity items in PPP [35]. The STD values of the differences between the CLK93 clocks and the GBM final clocks for quad-system are illustrated in Fig. 2 and the average STD values for each system are shown in Table 1. It is clear that the GPS and Galileo satellite clocks agree well with the final clocks and their STD values are around 0.1 ns. The clock accuracy of GLONASS is about 0.2 ns, which is twice worse than that of GPS/Galileo and the BDS-2 clock accuracy is the lowest with 0.3 ns of all systems. The STD results of the four systems are almost the same accuracy as those indicated by [35].

4 Experiment with MGEX data

To investigate and compare the performance of three widely used RT-SFPPP models, GPS, GLONASS, BDS-2 and Galileo observation data sampled at 30 s were collected from 16 MGEX stations, which covered a ten-day period of DOY 121–130 in 2019. These selected stations are globally distributed and shown in Fig. 3. Table 2 presents the receiver and antenna information of six receiver types involved in this experiment. It is worth noting that the data sets were collected in the post mode, while the SFPPP was simulated in RT mode.

4.1 Processing strategy

The Net_Diff software (http://202.127.29.4/shao_gnss_ac/Net_diff/Net_diff.html) is utilised to carry out multi-GNSS RT-SFPPP in the kinematic modes [36–37]. The detailed data processing strategies and adopted models for quad-system positioning are presented in Table 3. To maintain the consistency of the code and phase observations of quad-systems, the SF1 and SF2 are used to denote observations on the first and the second frequency, respectively. In this contribution, the stochastic model of the observations is represented by a sine function based on the elevation angle of the
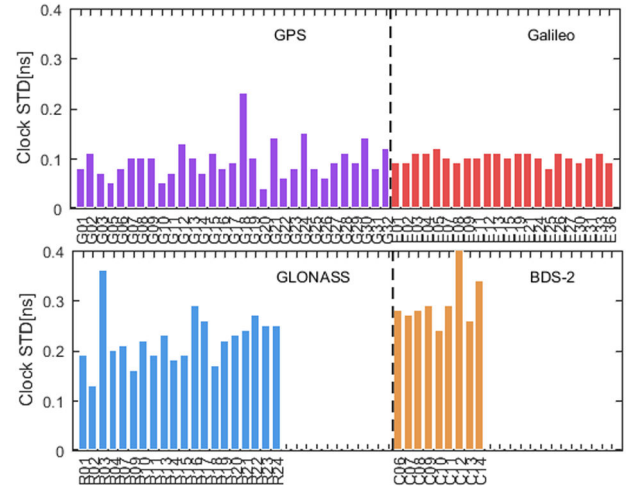

Fig. 2 *STD values of the differences between CLK93 clocks and GBM final clocks for the GPS, GLONASS, BDS-2 and Galileo*

Fig. 3 *Distribution of the selected 16 global MGEX tracking stations*

Table 2 Station information for the test of multi-GNSS RT-SFPPP

Station	Location	Receiver	Antenna
BSHM	Israel	Javad TRE_3	TRM59800.00
LEIJ	Germany	Javad TRE_3	LEIAR25.R3
POL2	Kyrgyzstan	Javad TRE_3	TPSCR.G3
GRAZ	Austria	Sept Polarx5	LEIAR25.R4
YEL2	Canada		
HARB	South Africa	Sept Polarx5	TRM59800.00
HOB2	Australia	Sept Polarx5	AOAD/M_T
TID1	Australia		
KAT1	Australia	Sept Polarx5	LEIAR25.R3
KOUG`	French Guiana		
YARR	Australia	Sept Polarx5	LEIAT504
PALM	Palmer Station	Javad TRE_G3TH	ASH700936D_M
PIE1	America	Javad TRE_G3TH	ASH701945E_M
HKSL	China	Leica GR50	LEIAR25.R4
MAJU	Marshall Islands	Sept Polarx4	JAVRINGANT_DM
GMSD	Japan	Trimble NetR9	TRM59800.00

satellite. The priori precision of the GPS/Galileo code and phase observations is set to 0.3 and 0.003 m, respectively [38–39]. Due to the low accuracy of RT orbit and clock products, the priori precision of the GLONASS observations needs to be set as twice as that of GPS, while for BDS, the priori precision is set as four times as that of GPS. Noted that the IGS weekly solutions in solution-independent exchange (SINEX) format are employed as the reference coordinates in RT-SFPPP using MGEX stations [40].

Table 3 Adopted models and strategies for multi-GNSS RT-SFPPP

| Item	Models/strategies
frequency selection	GPS/GLONASS: L1/L2; BDS: B1/B2; Galileo: E1/E5a
elevation cut-off angle	10°
estimator	Kalman filter
satellite orbit and clock	CLK93 orbit and clock corrections + broadcast ephemeris
tropospheric delay	modified (GPT2w + SAAS + VMF [41]) for the dry part and estimated for a wet part as random-walk noise process
ionospheric delay	corrected by CNES VTEC products or estimated as random-walk noise process
receiver APC	PCO/PCV (phase centre variation) values for GPS and GLONASS from igs14.atx are used; corrections for BDS and Galileo are assumed the same with GPS
satellite APC	PCO/PCV values for GPS, GLONASS and Galileo from igs14.atx are used; BDS PCO corrected with the value released by ESA and PCV is not considered
differential code bias	correct using CLK93 bias products
tidal effects	consider solid tides, ocean loading and polar tides [42]
relativistic effects	corrected by model
phase windup	corrected by model
station reference coordinates	IGS SINEX solutions
station coordinates	estimated as white noises in the kinematic modes
receiver clock	estimated as white noise process
receiver ISB	set up for GLONASS/BDS/Galileo and estimated as a random-walk noise process
GLONASS code IFB	modelled as a linear function of channel numbers
phase ambiguities	estimated as float constants for each arc
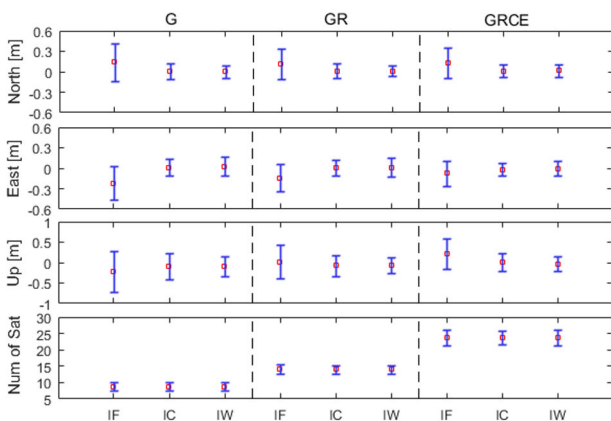
Fig. 4 *Comparison of SF1 kinematic positioning of RT-SFPPP with different schemes for single- and multi-GNSS solutions (station GMSD, on May 6, 2019). The abbreviation G, R, C and E represent GPS, GLONASS, BDS-2 and Galileo, respectively*

4.2 Positioning accuracy

Three RT-SFPPP models, i.e. IC, IF and IW, will be analytically compared for both single- and multi-GNSS by evaluating the positioning performance of their solutions. Fig. 4 shows the average positioning errors (red square) with the corresponding standard deviations (STD, blue error bar) based on three different models for GPS-only, GPS + GLONASS and GPS + GLONASS + BDS + Galileo solutions using station GMSD (DOY 126 in 2019) data. The threshold equal to 1.5 m of the STD of each component
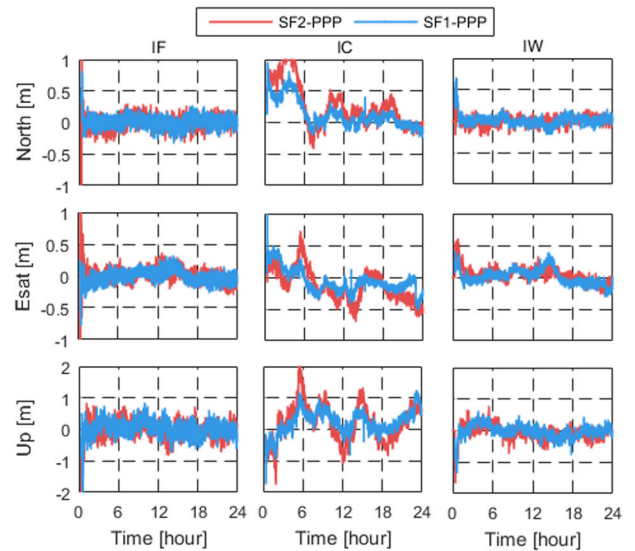
Fig. 5 *Comparison of kinematic positioning of GPS + GLONASS + BDS-2 + Galileo RT-SFPPP between SF1 and SF2 (station GMSD, on 6 May 2019)*

was employed to remove results during the initialisation period. We can see that the horizontal error of RT-SFPPP using CLK93 products is generally <0.6 m, while the vertical error is relatively larger. The RT-SFPPP based on the IC model shows the worst performances, especially in the *U* (Up) direction, mainly because of the limited accuracy of CNES VTEC products. Although the ionospheric errors can be removed in both IF and IW models, the IW model performs slightly better than the IF model. The main reason is that the IF combination introduces half of the code noise, which is much larger than the phase noise in the IW model. By integrating the multi-GNSS observations, the positioning accuracy of GPS-only RT-SFPPP is improved to some extent in three directions, which is reasonable as the number of visible satellites at each epoch are increased and position dilution of precision (PDOP) decreased.

The ionospheric delay, as a frequency-dependent error, has different effects on RT-SFPPP users with different frequency observations. The same station GMSD (DOY 126 in 2019) is used as an example, the SF1 and SF2 epoch-wise positioning errors of kinematic quad-system RT-SFPPP based on the three different models are given in Fig. 5. Obviously, compared with IF and IW models, the 24-h results of IC model are significantly different in SF1 and SF2 solutions. This is due to the fact that the ionospheric error of SF2 is amplified on the second frequency, which caused larger observation residuals of SF2. As for IF and IW models, however, this amplification has little effect on the positioning performance.

The single- and multi-GNSS kinematic positioning accuracies for daily solutions of IC, IF and IW models on all days over all the test stations are summarised in Table 4. It can be seen that the positioning accuracy of IW model in the N (north), E (east) and *U* directions is better than that of IC and IF models for all systems. Both IF and IW models show similar accuracy for SF1 and SF2 solutions, while their three-dimensional (3D) RMS accuracy difference is more than 0.3 m for the IC model. By introducing the quad-system observations, positioning accuracy of RT-SFPPP is improved as expected. Compared to the GPS-only solutions, for instance, the SF1 RT-SFPPP 3D positioning accuracy is improved by 9.7/12.2/5.7, 5.8/1.7/1.4 and 7.3/4.5/8.3% for the IC/IF/IW solutions with the dual-system combinations of GPS + GLONASS, GPS + BDS-2 and GPS + Galileo, respectively. Among all dual-system solutions, the GPS + BDS-2 positioning accuracy is the worst and performs almost the same as GPS-only. One reason is that the accuracy of RT orbit and clock products for BDS-2 is lower than other systems, the other point is that only nine BDS-2 satellites (C06-C14) are available in the test period and the improvement of PDOP is limited. When GPS, GLONASS, BDS-2 and Galileo observations are combined at the same time, the

Table 4 RMS of SF1 and SF2 positioning errors for single- and multi-GNSS with three RT-SFPPP models in the kinematic mode (in cm)

System	Model	SF1				SF2			
		N	E	U	3D	N	E	U	3D
G	IW	13.5	15.6	28.3	35.1	14.8	16.3	28.2	35.7
G	IF	16.8	16.4	35.4	42.5	18.1	18.3	33.8	42.4
G	IC	25.9	31.7	57.1	70.2	40.3	50.2	85.9	107.4
GR	IW	12.9	14.6	26.8	33.1	14.3	15.4	26.1	33.5
GR	IF	14.8	14.4	31.1	37.3	15.6	15.5	29.5	36.9
GR	IC	25.0	29.4	50.4	63.4	36.6	45.4	72.0	92.7
GC	IW	13.2	15.6	27.9	34.6	14.6	16.2	27.8	35.2
GC	IF	16.2	15.7	35.2	41.8	17.5	17.9	33.1	41.4
GC	IC	26.6	29.1	53.1	66.1	41.2	44.9	76.3	97.6
GE	IW	11.6	13.5	26.9	32.2	12.8	14.9	26.7	33.1
GE	IF	15.9	15.8	33.9	40.6	16.7	17.3	33.2	41.1
GE	IC	24.9	30.4	51.9	65.1	39.0	48.9	77.3	99.3
GRCE	IW	11.6	13.5	24.4	30.1	11.5	13.3	23.7	29.6
GRCE	IF	14.1	13.5	30.5	36.2	14.2	14.3	29.4	35.6
GRCE	IC	24.7	27.4	47.4	60.0	36.2	41.8	66.6	86.5

positioning accuracy of RT-SFPPP will be further improved. The IC model with quad-system observations can obtain the RMS accuracy of <0.3 m in horizontal and 0.5 m in vertical, which is much better than that of GPS + GLONASS results in [13]. As to the IF/IW model, the RMS of about 0.15/0.14 m in horizontal and 0.30/0.25 m in vertical will be achieved.

4.3 Observation residuals

To verify and explain the positioning performance of IC, IF and IW models, the observation residuals can be further analysed [43]. Generally, the unmodelled errors such as measurements noises and residual ionospheric delays are contained in the observation residuals of RT-SFPPP. To be consistent with the 24-h results in Section 4.1, the station GMSD (DOY 126 in 2019) is employed as an example, the distribution of its epoch-wise quad-system code and phase observation residuals for IC, IF and IW kinematic RT-SFPPP is shown in Fig. 6. For the three models, both code and phase observation residuals exhibit approximately normal distribution and their statistical results in terms of mean value and RMS value are also provided in each panel. Since the raw observations have the smallest noise in IW model, their average residuals and RMS are significantly smaller than those of both IC and IF models. This also explains the best RT-SFPPP positioning accuracy of IW model. It is interesting that the RMS value of phase observation residuals in IW model is <0.5 mm, which is much smaller than the theoretical noise level of raw phase observation (i.e. 3.0 mm). The results indicate that most of unmodelled errors in IW model can be absorbed into the ionospheric delay parameters, which are estimated as a random-walk noise process in this study. For the code observation residuals, the IC and IF models perform a comparable performance and their RMS of SF2 are larger than those of SF1, which is caused by the amplification of the residual ionospheric delays. As to the phase observation residuals, the RMS of the IC model is two to three times larger than that of the IF model, which contains half of code and phase noises but without the residual ionospheric delays.

4.4 Convergence analysis

Another indicator for the evaluation of RT-SFPPP models is the (re-)convergence time. The data at station LEIJ (DOY 126 in 2019) was selected to compare the convergence performance of IC, IF and IW models, their positioning errors of kinematic RT-SFPPP with quad-system observations are shown in Fig. 7. The simulated signal interruptions are introduced every 6 h by adding a new set of ambiguities for all available satellites, and all other estimated parameters are kept in the positioning filter with their covariances from the previous epoch. It can be seen that the convergence performance of the IW model is much shorter, and there is no

visible discontinuity in case of interruption. The major reason is that the ionospheric effect is adequately compensated by applying proper priori constraint in IW model. The position time series of IF model after each interruption shows significant discontinuity, which usually takes around 20–30 min for re-convergence. Although the results of IC model perform similar fluctuations in the whole time series, its amplitude is smaller and the re-convergence time is shorter than that of IF model, which is mainly attributed to the high-precision CNES VTEC products and smaller raw observations noises.

Fig. 8 shows the average convergence time of SF1 and SF2 kinematic RT-SFPPP with different schemes for all 16 stations in a ten-day period. Here, 2D represents that the convergence condition of both N and E components are <0.5 m and keep within 0.5 m for >30 consecutive epochs, while for 3D represents that besides the former condition, the U component is <1.0 m for 30 continuous epochs. The convergence time is the period from the first epoch to the converged epoch. It should be noted that the results of the IC model are excluded since they cannot meet the requirements of the convergence condition. We can see that the convergence time of the IW model is much shorter than that of the IF model for all single- and multi-GNSS solutions. As to the results of different frequencies, the IW model of both SF1 and SF2 perform similarly, while the IF model of SF2 shows slightly worse performance than that of SF1. The reason for this situation is that the ionospheric errors of SF2 are amplified, which leads to relatively larger code observation residuals in the IF model of SF2. The convergence time of both IF and IW models can be shortened by integrating the multi-GNSS observations. Compared with GPS-only solution, the average 3D convergence time of quad-system IF/IW RT-SFPPP is of 39.9/31.3 and 46.3/38.1% for SF1 and SF2. The average 3D convergence time of quad-system IW model is of 24.8 and 24.1 min for SF1 and SF2, which is 26.2 and 28.9% shorter than the IF model.

5 Experiment with shipborne GNSS data

To further compare and evaluate the performance of kinematic multi-GNSS RT-SFPPP with different models, a true RT kinematic test based on shipborne data and CLK93 products was conducted in Tokyo Bay, Japan, on 15 January 2020. Fig. 9 shows the rover trajectory during the testing period from GPST 00:47:19 to 05:55:49. The GNSS receiver of the reference and rover used for the experiment were TRIMBLE NETR9 and TRIMBLE SPS855, which collects the GPS, GLONASS, BDS-2, Galileo and QZSS observations with the sampling interval of 1 s. The reference coordinates of the rover are generated by the carrier-phase-based double-differenced real-time kinematic (RTK) with five-system using the Net_Diff software, with a positioning accuracy of 3–4 cm in the horizontal and vertical components [44].
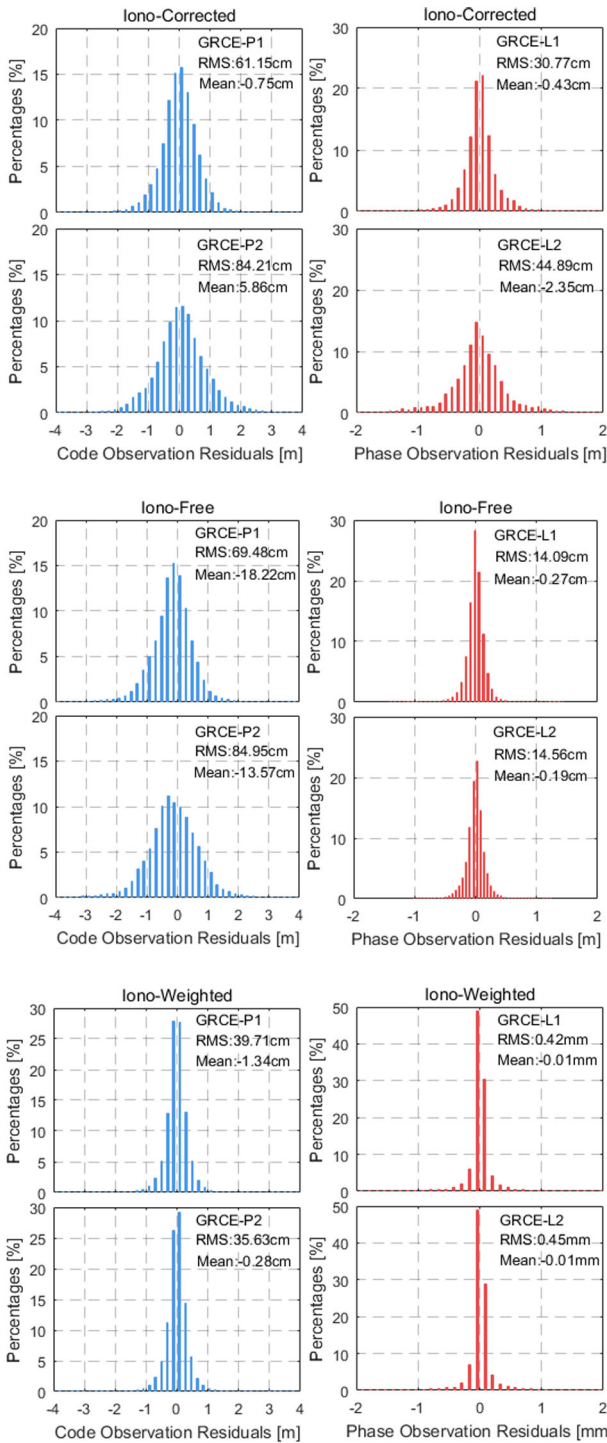
Fig. 6 *Distribution of epoch-wise kinematic RT-SFPPP code and phase observation residuals for IC, IF and IW models with quad-system observations (station GMSD, on 6 May 2019)*

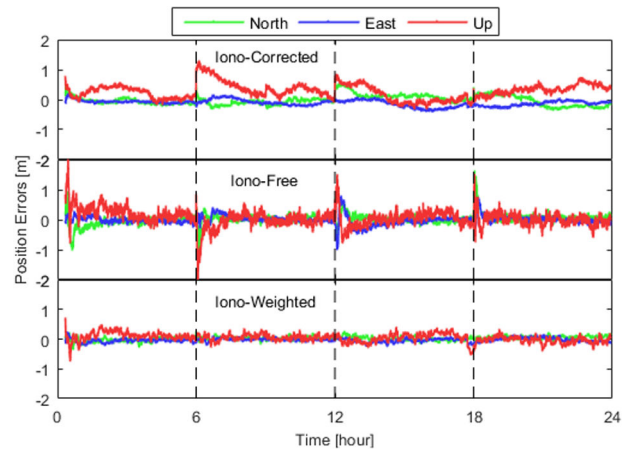**Fig. 7** *Positioning errors of SF1 kinematic GPS + GLONASS + BDS-2 + Galileo RT-SFPPP based on IC, IF and IW models (station LEIJ, on 6 May 2019)*
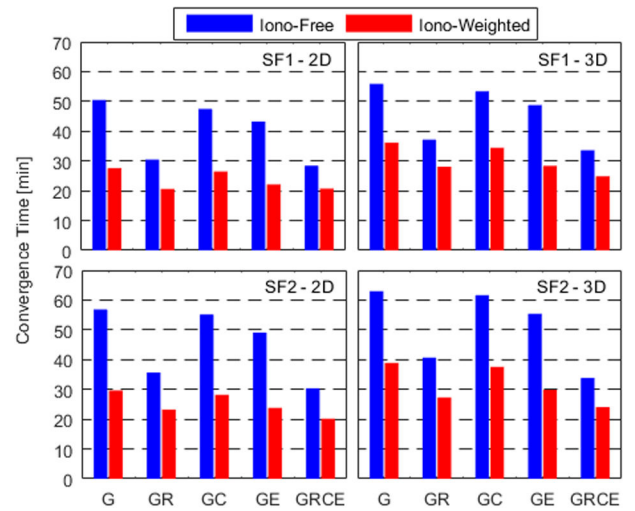

Fig. 8 *Average convergence time of kinematic RT-SFPPP based on IF and IW models for single- and multi-GNSS solutions*
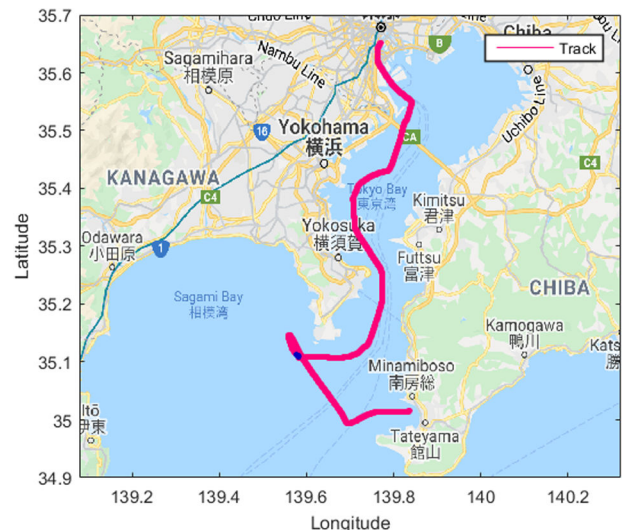

Fig. 9 *Ship trajectory of the kinematic multi-GNSS RT-SFPPP test (Tokyo Bay, Japan)*

In the following calculations, the same processing strategies and settings in Table 3 are employed. Noted that only the GPS + GLONASS + BDS-2 RT-SFPPP was performed due to the absence of Galileo orbit and clock products from the CLK93 stream during the testing period. Since the IF model is dominated by the code noise, an RT single-frequency code noise and multipath correction filter is applied to smooth the code observations in this experiment [45]. Fig. 10 illustrates the time series of SF1 positioning errors in the *N*, *E* and *U* directions for the three kinematic RT-SFPPP models. The number of tracked satellites and the corresponding PDOP are shown in Fig. 11. Regarding the positioning accuracy, both IF and IW models show similar performance and are much better than IC model in the *U* direction, and the RMS errors in horizontal and vertical are <0.3 and 0.5 m, respectively. The satellite signals were blocked by the bridge at the GPST 00:58:31

to 00:58:37 (Fig. 12), the number of tracked satellites was dropped significantly and results in a visible discontinuity in both IC and IF models. By contrast, no re-convergence occurs for the IW model, which improves the continuity of kinematic RT-SFPPP. In addition, with Galileo satellites to be used, better RT-SFPPP positioning performance is expected to be achieved in this experiment.
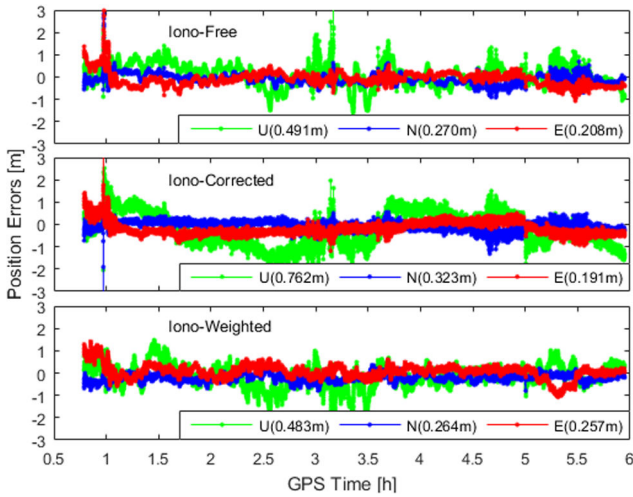
1732

Fig. 10 *Positioning errors with IC, IF and IW RT-SFPPP models for GPS + GLONASS + BDS solution in the kinematic mode*
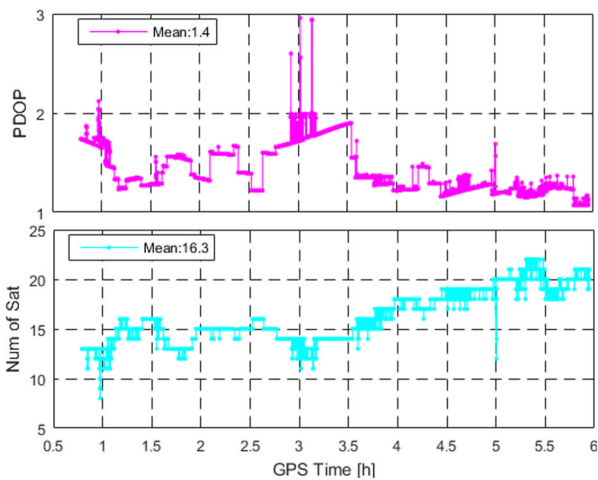

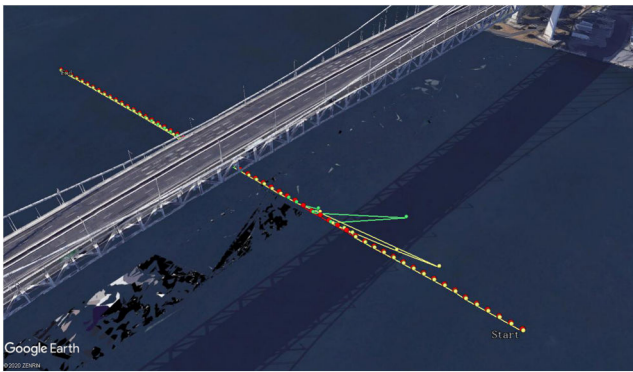**Fig. 11** *Number of tracked satellites and the corresponding PDOP values*

Fig. 12 *Ship trajectory of kinematic RT-SFPPP using IC (green), IF (yellow) and IW (red) models during the test period of GPST 00:58:00–00:58:59*

6 Conclusions

With the increasing demand for real-time, low-cost and high-precision applications, RT-SFPPP using the IGS RTS has attracted more attention from GNSS users. This contribution focuses on a comprehensive comparison among three widely used RT-SFPPP models, i.e. IC, IF and IW, using RTS CLK93 products as inputs. The ten-day data of 16 MGEX stations and 5-h shipborne are processed in kinematic RT-SFPPP and results are discussed in terms of observation residuals, positioning accuracy and convergence time. The research findings are summarised as follows:

(i) Both code and phase observation residuals of IW model are significantly smaller than those of IC and IF models. The ionospheric delay parameters estimated as a random-walk noise process in IW model can absorb parts of unmodelled errors.
(ii) The positioning performance of SF1 in IC model is better than that of SF2, due to the amplified ionospheric error of SF2. However, this amplification has little effect on IF and IW models.
(iii) The IW model performs faster convergence than that of IF model, while the IC model is difficult to converge to the decimetre-level positioning accuracy. In case of interruption, there is no coordinate discontinuity for IW RT-SFPPP. The convergence time of IW model is shortened by at least 25% compared with IF model.
(iv) Based on the quad-system observations of static MGEX stations, the RMS of IW and IF models can achieve 0.15 m in horizontal and 0.30 m in vertical. However, the IC model with quad-system observations obtains 0.3 and 0.5 m accuracies in the horizontal and vertical components, respectively. Regarding the shipborne experiment, the positioning accuracy of IF/IW model is 0.27/0.26, 0.21/0.26 and 0.49/0.48 m in the *N*, *E* and *U* components, respectively, which is much better than that of IC model.

In summary, the IW model using CNES VTEC products has the best positioning performance for all situations and is recommended for high-precision RT-SFPPP users.

7 Acknowledgments

8 References

[1] Caissy, M., Agrotis, L.: 'Real-time working group and real-time pilot project', Int GNSS Serv Tech Rep, 2011, pp. 183–190
[2] Hadas, T., Bosy, J.: 'IGS RTS precise orbits and clocks verification and quality degradation over time', *GPS Solut.*, 2015, **19**, (1), pp. 93–105
[3] Chen, J., Li, H., Wu, B., *et al.*: 'Performance of real-time precise point positioning', *Mar. Geod.*, 2013, **36**, (1), pp. 98–108
[4] Kazmierski, K., Sosnica, K., Hadas, T.: 'Quality assessment of multi-GNSS orbits and clocks for real-time precise point positioning', *GPS Solut.*, 2018, **22**, p. 11
[5] van Bree, R.J., Tiberius, C.C.J.M.: 'Real-time single-frequency precise point positioning: accuracy assessment', *GPS Solut.*, 2012, **16**, (2), pp. 259–266
[6] de Bakker, P.F., Tiberius, C.C.J.M.: 'Real-time multi-GNSS single-frequency precise point positioning', *GPS Solut.*, 2017, **21**, pp. 1791–1803
[7] Klobuchar, J.: 'Ionospheric time-delay algorithm for single-frequency GPS users', *IEEE Trans. Aerosp. Electron. Syst.*, 1987, **23**, pp. 325–331
[8] Bidaine, B.: 'Ionosphere modelling for Galileo single frequency users', Ph.D Thesis, University of Liege, Liege, Belgium, 2012
[9] Angrisano, A., Gaglione, S., Gioia, C., *et al.*: 'Benefit of the NeQuick galileo version in GNSS single-point positioning', *Int. J. Navig. Obs.*, 2013, **302947**, doi: 10.1155/2013/302947
[10] European GNSS (Galileo) Open Service.: 'Ionospheric correction algorithm for galileo single frequency users', (1.1), June 2015
[11] Hoque, M., Jakowski, N.: 'An alternative ionospheric correction model for global navigation satellite systems', *J. Geodesy*, 2015, **89**, (4), pp. 391–406
[12] Yuan, Y., Wang, N., Li, Z., *et al.*: 'The BeiDou global broadcast ionospheric delay correction model (BDGIM) and its preliminary performance evaluation results', *Navigation*, 2019, **66**, (1), pp. 55–69
[13] Nie, Z., Yang, H., Zhou, P., *et al.*: 'Quality assessment of CNES real-time ionospheric products', *GPS Solut.*, 2019, **23**, p. 11
[14] Liu, T., Wang, J., Yu, H., *et al.*: 'A new weighting approach with application to ionospheric delay constraint for GPS/GALILEO real-time precise point positioning', *Appl. Sci.*, 2018, **8**, p. 2537
[15] Yunck, T.P..: 'Coping with the atmosphere and ionosphere in precise satellite and ground positioning', In: Vallance-Jones, A. (Ed.): '*Environmental effects on spacecraft positioning and trajectories*' (American Geophysical Union (AGU), USA, 1993), **73**, (13), pp. 1–16
[16] Cai, C., Liu, Z., Luo, X.: 'Single-frequency ionosphere-free precise point positioning using combined GPS and GLONASS observations', *J. Navig.*, 2013, **66**, (3), pp. 417–434
[17] Shi, C., Gu, S., Lou, Y., *et al.*: 'An improved approach to model ionospheric delays for single-frequency precise point positioning', *Adv. Space Res.*, 2012, **49**, pp. 1698–1708

[18]   Li, B., Zang, N., Ge, H.*, et al.*: 'Single-frequency PPP models: analytical and numerical comparison', *J. Geod.*, 2019, **93**, pp. 2499–2514

[19]   Hoffmann-Wellenhof, B., Lichtenegger, H., Collins, J.: '*Global positioning system: theory and practice*' (Springer, New York, 1992)

[20]   Shi, C., Yi, W., Song, W.*, et al.*: 'GLONASS pseudorange inter-channel biases and their effects on combined GPS/GLONASS precise point positioning', *GPS Solut.*, 2013, **17**, pp. 439–451

[21]   Ghoddousi-Fard, R., Lahaye, F.: 'Evaluation of single frequency GPS precise point positioning assisted with external ionosphere sources', *Adv. Space Res.*, 2016, **57**, (10), pp. 2154–2166

[22]   Paziewski, J., Wielgosz, P.: 'Accounting for Galileo-GPS inter-system biases in precise satellite positioning', *J. Geod.*, 2015, **89**, pp. 81–93

[23]   Afifi, A., El-Rabbany, A.: 'An improved model for single-frequency GPS/galileo precise point positioning', *Positioning*, 2015, **6**, pp. 7–21

[24]   Gioia, C., Borio, D.: 'A statistical characterization of the galileo-to-GPS inter-system bias', *J. Geod.*, 2016, **90**, pp. 1279–1291

[25]   Gioia, C., Pisoni, F., Fortuny, J.: 'Estimation of the GPS to galileo time offset and its validation on a mass market receiver'. Seventh ESA workshop on GNSS signals and signal processing (NAVITEC), Nijmegen, the Netherlands, 2014

[26]   Su, K., Jin, S., Hoque, M.M.: 'Evaluation of ionospheric delay effects on multi-GNSS positioning performance', *Remote Sens.*, 2019, **11**, p. 171

[27]   Wang, A., Chen, J., Zhang, Y.*, et al.*: 'Performance of selected ionospheric models in multi-global navigation satellite system single-frequency positioning over China', *Remote Sens.*, 2019, **11**, p. 2070

[28]   RTCM Special Committee.: 'RTCM standard 10403.3 differential GNSS (global navigation satellite systems) services-version 3', RTCM Special Committee No.104, Arlington, TX, USA, 2016

[29]   Deng, Z., Fritsche, M., Uhlemann, M.*, et al.*: 'Reprocessing of GFZ multi-GNSS product GBM', IGS Workshop 2016, Sydney, 2016

[30]   EI-Mowafy, A., Deo, M., Kubo, N.: 'Maintaining real-time precise point positioning during outages of orbit and clock corrections', *GPS Solut.*, 2017, **21**, (3), pp. 937–947

[31]   Montenbruck, O., Steigenberger, P., Hauschild, A.: 'Multi-GNSS signal-in-space range error assessment-methology and results', *Adv. Space Res.*, 2018, **61**, pp. 3020–3038

[32]   Zhang, Y., Kubo, N., Chen, J.*, et al.*: 'Initial positioning assessment of BDS new satellite and new signal', *Remote Sens.*, 2019, **11**, (11), p. 1320

[33]   Wang, L., Li, Z., Ge, M.*, et al.*: 'Investigation of the performance of real-time BDS-only precise point positioning using the IGS real-time service', *GPS Solut.*, 2019, **23**, p. 66

[34]   Kazmierski, K., Hadas, T., Sosnica, K.: 'Weighting of multi-GNSS observations in real-time precise point positioning', *Remote Sens.*, 2018, **10**, p. 84

[35]   Lu, C., Chen, X., Liu, G.*, et al.*: 'Real-time tropospheric delays retrieved from multi-GNSS observations and IGS real-time product streams', *Remote Sens.*, 2017, **9**, p. 1317

[36]   Chen, J., Wang, A., Zhang, Y.*, et al.*: 'BDS satellite-based augmentation service correction parameters and performance assessment', *Remote Sens.*, 2020, **12**, p. 766

[37]   Zhang, Y., Chen, J., Gong, X.*, et al.*: 'The update of BDS-2 TGD and its impact on positioning', *Adv. Space Res.*, 2020, **65**, (11), pp. 2645–2661

[38]   Kiliszek, D., Kroszczynski, K.: 'Performance of the precise point positioning method along with development of GPS, GLONASS and galileo systems', *Measurement*, 2020, **164**, p. 108009

[39]   Zhou, F., Dong, D., Li, P.*, et al.*: 'Influence of stochastic modeling for inter-system biases on multi-GNSS undifferenced and uncombined precise point positioning', *GPS Solut.*, 2019, **23**, p. 59

[40]   Johnston, G., Riddell, A., Hausler, G.: 'The International GNSS Service', In Teunissen Peter, J.G., Montenbruck, O. (Eds.): '*Springer handbook of global navigation satellite systems*' (Cham, Switzerland, 2017), pp. 967–982

[41]   Boehm, J., Moller, G., Schindelegger, M.*, et al.*: 'Development of an improved empirical model for slant delays in the troposphere (GPT2w)', *GPS Solut.*, 2015, **19**, pp. 433–441

[42]   Gerard, P., Luzum, B.: 'IERS conventions', IERS Technical 2010 Note 36. Verlag des Bundesamts für Kartographie und Geodäsie, Frankfurt am Main, Germany, 2010

[43]   Pan, L., Zhang, X., Liu, J.: 'A comparison of three widely used GPS triple-frequency precise point positioning models', *GPS Solut.*, 2019, **23**, p. 121

[44]   Zhang, Y., Kubo, N., Chen, J.*, et al.*: 'Contribution of QZSS with four satellites to multi-GNSS long baseline RTK', *J. Spatial Sci.*, 2019, **65**, (1), pp. 41–60

[45]   Chang, Z., Hu, X., Guo, R.*, et al.*: 'Comparison between CNMC and hatch filter & its precision analysis for BDS precise relative positioning (in Chinese)', *Scientia Sinica Physica, Mechanica & Astronomica*, 2015, **45**, (7), p. 079508